HHS Public Access

Author manuscript

Nat Neurosci. Author manuscript; available in PMC 2012 January 01.

Published in final edited form as:

Nat Neurosci. ; 14(7): 866–873. doi:10.1038/nn.2837.

Unique functions of kainate receptors in the brain are determined by the auxiliary subunit Neto1

Christoph Straub[1,2,5], **David L. Hunt**[3,5], **Miwako Yamasaki**[4], **Kwang S. Kim**[1,2], **Masahiko Watanabe**[4], **Pablo E. Castillo**[3,*], and **Susumu Tomita**[1,2,*]

[1]Program in Cellular Neuroscience, Neurodegeneration and Repair, Yale University School of Medicine, New Haven, CT 06520

[2]Department of Cellular and Molecular Physiology, Yale University School of Medicine, New Haven, CT 06520

[3]Dominick P. Purpura Department of Neuroscience, Albert Einstein College of Medicine, Bronx, NY10461

[4]Department of Anatomy, Hokkaido University Graduate School of Medicine, Sapporo 060-8638, Japan

Abstract

Ionotropic glutamate receptors principally mediate fast excitatory transmission in the brain. Among the three classes of ionotropic glutamate receptors, kainate receptors (KARs) display a categorical brain distribution, which has been historically defined by ^{3}H-radiolabeled kainate binding. Compared with recombinant KARs expressed in heterologous cells, synaptic KARs exhibit characteristically slow rise-time and decay kinetics. However, the mechanisms responsible for these unique KAR properties remain unclear. Here we found that both the distinct high affinity biding pattern in the mouse brain and the channel properties of native KARs are determined by the KAR auxiliary subunit Neto1. Through modulation of agonist binding affinity and off-kinetics of KARs, but not trafficking of KARs, Neto1 determines both KAR high affinity binding pattern and the distinctively slow kinetics of postsynaptic KARs. By regulating KAR-EPSC kinetics, Neto1 can control synaptic temporal summation, spike generation and fidelity.

Fast excitatory synaptic transmission in the vertebrate brain is predominantly mediated by three classes of ionotropic glutamate receptors: AMPA (α-amino-3-hydroxy-5-methyl-4-isoxazole propionic acid) receptors (AMPARs), NMDA (N-methyl-d-aspartate) receptors (NMDARs), and kainate receptors (KARs). AMPARs mediate fast synaptic transmission

*To whom correspondence should be addressed: Yale University School of Medicine, 295 Congress Ave BCMM441, PO Box 208026, New Haven, CT 06510, Susumu.Tomita@yale.edu; Dominick P.Purpura Department of Neuroscience, Albert Einstein College of Medicine, 1410 Pelham Parkway South, Kennedy Center, Room 703, Bronx, NY10461, Pablo.Castillo@einstein.yu.edu.

[5]These authors contributed equally to this work.

Author Contributions. S.T. and P.E.C. conceived the project and wrote the manuscript. C.S., D.L.H., M.Y., K.S.K., M.W. and S.T. performed all of the experiments and analyzed results. All authors, CS and DLH in particular, contributed to the final version of the manuscript.

whereas NMDARs classically induce synaptic plasticity. While the role of KARs is less understood, these receptors mediate both synaptic transmission and plasticity (for recent reviews, see[1-5]). Notably, KARs show a distinct expression pattern unlike AMPARs and NMDARs, which are found ubiquitously in the brain. *In-vitro* autoradiographic techniques with [^{3}H]-radiolabeled kainate have shown uniquely strong [^{3}H]kainate signals at the hippocampus *s. lucidum* – where mossy fiber to CA3 pyramidal cell synapses are found –, cerebral cortex, striatum, and cerebellar granule cell layer[6]. The mechanistic basis for this unique distribution of high affinity KARs in the brain is unknown.

Neuronal KARs mediate a characteristically slow EPSC (KAR-EPSC), which was originally identified at the mossy fiber to CA3 synapse (mf-CA3)[7, 8] and has been demonstrated at other central synapses[9-16]. When compared with AMPAR-EPSCs, the slow KAR-EPSCs provides a crucial synaptic mechanism for encoding temporal information[17]. In this way KARs can control spike transmission[18] and network activity[19]. Intriguingly, the slow kinetics of *native* KARs clearly contrasts the fast activation, deactivation and desensitization of *recombinant* KARs. For example, while synaptic KARs typically show relatively slow decay time constants[7, 9, 20], recombinant KARs desensitize/deactivate in a few milliseconds[21-30]. While the underlying explanation for this major discrepancy between recombinant and native KARs is unclear, a number of studies have attempted to pinpoint the molecular substrates that cause this disparity. Several candidate KAR interacting molecules, including PSD-95, PICK1, GRIP, KRIP6, cadherin/catenin, and Neto2, have been identified[31-35]. However, most of these studies have been performed using expression systems, and as a result, the molecular substrate controlling the slow kinetics of native KARs in the brain remains elusive.

Here we found that the unique distribution of KARs labeled with [^{3}H]kainate at the hippocampal *s. lucidum* is determined by the KAR auxiliary subunit, Neto1 at postsynapses. Neto1 interacted with KARs *in vivo*, and Neto1 expression was reduced in the hippocampus from GluK2-knockout mice. In Neto1-knockout mice, we observed a selective reduction in the amplitude and decay kinetics of mf-CA3 KAR-EPSCs, which reconciles the difference in channel kinetics between native and recombinant KARs. Neto1 has been recently identified as an NMDAR-interacting protein regulating NMDAR function[36]. Unexpectedly, we found no biochemical and functional interactions between Neto1 and NMDARs. Moreover, presynaptic function remained unchanged in Neto1-knockout mice. Thus, our results indicate that two unique properties of native KARs, namely, their high affinity-binding pattern in the brain and their distinct slow kinetics at postsynapses, are endowed by the KAR auxiliary subunit Neto1.

Results

Hippocampus-abundant Neto1 interacts with kainate receptors *in-vivo*

To investigate the molecular mechanisms underlying the unique distribution of KARs typically revealed by [^{3}H]kainate binding pattern, particularly in the hippocampal *s. lucidum*, we first examined protein expression levels of the major KAR isoform GluK2/3 and the KAR auxiliary subunit Neto2[33, 37], which could potentially influence the KAR binding pattern. While GluK2/3 subunits are expressed in the hippocampus, Neto2 was

poorly expressed relative to other brain regions (Fig. 1a), making Neto2 an unlikely candidate mediating KAR localization in the hippocampus. Therefore, we subsequently examined expression of Neto1, which shares 80% similarity in amino acid sequence with Neto2, using specific antibodies to each Neto-isoform (Supplementary Fig. 1a,b). Notably, we found that Neto isoforms show a complementary expression pattern in the mouse brain (Fig. 1a). Neto1 is highly expressed in the hippocampus, whereas Neto2 is expressed strongly in most brain regions except the hippocampus (Fig. 1a). To test the interaction between Neto1 and KARs, we co-immunoprecipitated rat brain lysates with Neto isoform-specific antibodies. Both Neto1 and Neto2 co-immunoprecipitated with both GluK2/3 and GluK5 KAR subunits, but not with GluA1 AMPARs or PSD-95 (Fig. 1b). We consequently examined Neto1 expression in the total lysate and the PSD fraction of hippocampi from GluK2-knockout mice. We found that Neto1 expression was reduced in both the total lysate and the PSD fraction of the hippocampi from GluK2-knockout mice, without changes in AMPARs, NMDARs, or PSD-95 (Fig. 1c, d). Furthermore, we did not detect accumulation of Neto1 protein in GluK2-knockout mice (Supplementary Fig. 1c). From these results, we conclude that Neto1 specifically interacts with KARs in the brain.

Distinct distribution of high-affinity kainate receptors is determined by Neto1

The KAR auxiliary subunit Neto1 is strongly expressed in the hippocampus (Fig. 1a), particularly in the hippocampal *s. lucidum* (Supplementary Fig. 1c), where strong [^{3}H]kainate binding has been detected[6]. To reveal the roles of Neto 1 we generated Neto1 knockout mice. We obtained Neto1-targeted ES cells and germline-transmitted (Neto1-knockout) mice from a trans-NIH initiative, The Knockout Mouse Project (KOMP, www.komp.org). In this line of Neto1-knockout mice, the Neto1 gene was replaced with the beta-galactosidase gene. Endogenous Neto1 promoter-driven beta-galactosidase activity was strongest in hippocampal CA3 *s. pyramidale*, and modest in cerebral cortex, striatum, and hippocampal CA1 cells, as shown in the Neto1-knockout mice (Fig. 2a), which is consistent with the Neto1 *in situ* hybridization pattern[36, 38]. The expression of KARs (GluK2/3, GluK5) and other synaptic proteins, including AMPA and NMDA receptors (GluA2/3, GluN1, GluN2A, GluN2B) and PSD-95, were not altered in Neto1-knockout mice (Supplementary Fig. 2a). In addition, a specific interaction between Neto1 and KARs (GluK2/3 and GluK5) was confirmed by co-immunoprecipitation with the anti-Neto1 antibody using the brain lysate from wild-type and Neto1-knockout mice (Supplementary Fig. 2b). Next, we confirmed the distribution of Neto1 proteins in the brain by immunostaining with an anti-Neto1 antibody (Fig. 2b). Neto1 protein was strongly expressed in hippocampal *s. lucidum*, supporting the notion that Neto1 plays a role in defining the unique distribution of KARs as shown by [^{3}H]kainate labeling.

We examined [^{3}H]kainate binding in the hippocampus from wild-type, GluK2 knockout, and Neto1 knockout mice. Consistent with previous studies[6, 37], a strong signal was observed in the *s. lucidum* of wild type, but not GluK2-knockout mice (Fig. 3a). The [^{3}H]kainate signal was reduced in Neto1-knockout mice (Fig. 3a), suggesting that Neto1 regulates the binding of [^{3}H]kainate to high-affinity KARs. To measure the difference in kainate binding more quantitatively, we performed a biochemical binding assay using [^{3}H]kainate (100 nM) and hippocampal membranes from each genotype. The specific

[^{3}H]kainate signal was reduced nearly 80% in the hippocampus from GluK2-knockout mice compared to the signal in wild-type mice, indicating that GluK2 is required for most of kainate binding *in vivo* (WT 1533.2 ± 184.5 cpm; GluK2 KO 356.9 ± 91.1 cpm (n=9). p=0.00003)[37]. The GluK2-specific [^{3}H]kainate signal was reduced 50% in the Neto1-knockout relative to the wild type, (WT 1176.3 ± 116 cpm; Neto1 KO 544.2 ± 155.8 cpm, n=9 each, p=0.0048) without changes in the expression of KARs (Supplementary Fig. 2a). The remaining 50% could be due to residual Neto2 expression (Supplementary Fig. 2a) or to KARs that do not associate with Netos at pre- or post-synapses.

The high-affinity nature of KARs defined by [^{3}H]kainate labeling of brain sections could result from higher-affinity binding of kainate, or of slow off-kinetics of kainate from KARs[6, 39]. Accordingly, we examined the effects of Neto1 on the binding affinity and decay kinetics of KARs. The kainate-binding curve shifted noticeably in Neto1-knockout mice without changes in the expression of KARs (Fig. 3b and Supplementary Figs. 2a and 3a, b). The K_d for kainate calculated from the curve was 48.8 nM in the wild type and 202.6 nM in the Neto1-knockout (see methods). However, the value in the Neto1-knockout is likely to be an underestimation because the binding curve did not reach saturation. Although we could not estimate the K_d precisely, Neto1 clearly converts KARs into higher-affinity receptors. In addition, we examined the effects of Neto1 on the binding affinity of GluK2 KAR isoform expressed in HEK cells and found that the affinity curve of GluK2 shifted significantly by co-expression of Neto1 (Supplementary Fig. 3c).

To measure the effect of Neto1 on the off-kinetics of kainate from KARs, we measured the kainate-evoked decay kinetics of the KAR complex expressed in tsA201 cells using outside-out patch membranes and a piezoelectric device for ultrafast solution changes [33]. We adjusted the expression ratio of each protein component (GluK2, GluK5, and Neto1) in the transfected tsA201 cells to the ratio in the hippocampus lysate, although we expressed GluK5 more ensuring that we recorded mostly GluK2/5 heteromeric channels (Supplementary Fig. 3d). Under this condition, we found that Neto1 slowed both desensitization and deactivation of GluK2/GluK5 KAR heteromers, and increased the relative ratio of the steady-state and peak amplitudes 3-fold (Mock 2 + 0.45 %, n=7; Neto1 6.3 + 1.1 %, n=12, p=0.009) (Fig. 3c,d, and Supplementary Fig. 3e). Based on these observations, we postulate that high-affinity KARs in hippocampus likely contain Neto1, which modulates both the affinity of kainate for KARs and the off-kinetics. We also examined glutamate-evoked kinetics of the KAR/Neto1 complex expressed in tsA201 cells. As kainate-evoked kinetics, we found that Neto1 slowed both desensitization and deactivation of GluK2/GluK5 KAR heteromers, and accelerated recovery from desensitization (Supplementary Fig. 3f-i). These results suggest that Neto1 also modulates the KAR affinity for the endogenous ligand glutamate.

Neto1 modulates kainate receptor function in the hippocampus

To directly test whether loss of Neto1 affects KAR function, we first measured kainate-mediated currents in CA3 pyramidal cells, CA1 *s. radiatum* interneurons, and Purkinje cells in acute hippocampal and cerebellar slices of Neto1 wild-type and knockout mice. To this end, we bath applied 3 μM kainate, a relatively low concentration known to be specific for

KARs[37], and kainate-mediated currents were recorded in the presence of the AMPAR selective antagonist GYKI53655 (30 μM). Consistent with the expression of Neto1 in the hippocampus –at both pyramidal cells and inhibitory interneurons– but not in the cerebellum (Fig. 2a)[38], kainate-evoked inward currents were significantly reduced in CA3 pyramidal cells and CA1 interneurons, but not in Purkinje cells from Neto1-knockout mice (Fig. 4a-c). The reduction of KAR currents in CA3 pyramidal cells and CA1 interneurons from Neto1 knockout mice could be explained by either a decrease in KAR surface expression, or a decrease in channel activity. To distinguish between these two possibilities we examined KAR surface expression in acute hippocampal slices. Using a cell-impermeable biotinylated reagent[40], we confirmed the surface expression of KARs, but not the intracellular protein, tubulin, indicating that we were only detecting proteins at the cell surface (Fig. 4d). Utilizing this assay, we found no significant differences in the surface expression of GluK2/3 and GluK5 between wild-type and Neto1-knockout littermates (Fig. 4e). Consistent with this result, Neto1 did not increase surface expression of HA-tagged GluK2 in expressed heterologously in oocytes (Supplementary Fig. 3f). These results show that Neto1 modulates the channel properties, but not surface expression, of KARs. Moreover, the fact that Neto1 is predominantly expressed in CA3 pyramidal cells, at the *s. lucidum* in particular (Fig. 2a,b), and that [^{3}H]kainate signal is reduced in the CA3 *s. lucidum* of Neto1-knockout mice (Fig. 3a,b), strongly suggest that high-affinity, Neto1-associated KARs are localized at the mf-CA3 postsynaptic compartment.

The slow decay of kainate receptor-mediated EPSCs is determined by Neto1

Could the disparate decay kinetics between recombinant and native KARs be explained by Neto1? To address this question we monitored KAR-EPSCs in CA3 pyramidal cells[7, 8]. While mf-CA3 KAR-EPSCs were observed in both wild-type and Neto1-knockout mice, the KAR-EPSC decay kinetics and rise time from Neto1-knockout was much faster than from wild-type mice (Decay, WT Tau: 70 ± 3 ms, 8 cells, 4 animals; KO Tau = 17 ± 2 ms, 9 cells, 4 animals, p= 0.0038) (Rise time$_{10\text{-}90\%}$, WT: 2.7 ± 0.2 ms, 10 cells, 5 animals; KO = 1.6 ± 0.1 ms, 10 cells, 5 animals, p=0.00025) (Fig. 5,ba and Supplementary Fig. 4). In contrast, the decay kinetics of AMPAR- and NMDAR-EPSCs were not altered at associational/commissural–CA3 synapses (ac-CA3) and mf–CA3 synapses, respectively (AMPAR Decay, WT Tau: 13 ± 2 ms, 6 cells, 3 animals; KO Tau = 12 ± 2 ms, 6 cells, 3 animals, p= 0.1116) (NMDAR Decay, WT Tau: 86 ± 6 ms, 8 cells, 4 animals; KO Tau = 89 ± 6 ms, 8 cells, 4 animals, p= 0.8394) (Fig. 5c,d).

We next assessed whether Neto1 deletion affects the amplitude and relative contribution of the various glutamate receptor subtypes to glutamate receptor-mediated EPSCs. To compare the magnitude of these EPSCs across animals we calculated AMPAR/NMDAR and KAR/NMDAR EPSC ratios in wild-type and Neto1-knockout mice. By taking advantage of the use dependent blocker of NMDARs, MK-801, we determined the NMDAR mediated component of mf-CA3 EPSCs by holding CA3 pyramidal cells at +30mV in the presence of the AMPAR antagonist GYKI 53655 (30 μM). The synaptic current remaining in the presence of MK-801, which was sensitive to the KAR antagonist NBQX, was quantified as the KAR-mediated EPSC component. Following from this analysis, we found that the KAR/NMDAR ratio was reduced in Neto1-knockout mice relative to wild-type littermates, a

finding that could be due, at least in part, to Neto1-mediated changes in desensitization and/or deactivation of KARs (WT 0.17 ± 0.02 6 cells, 3 animals; KO 0.11 ± 0.02 6 cells, 3 animals, p=0.0214) (Fig. 5e) [33]. However, the AMPAR/NMDAR ratio was unchanged at ac-CA3 synapses (Ratio, WT 2.4 ± 0.2, 5 cells, 3 animals; KO 2.3 ± 0.2, 5 cells, 3 animals, p= 0.9291) (Fig. 5f) in contrast to a recent study showing a reduction of the NMDAR-mediated component at the functionally homologous Schaffer collateral to CA1 pyramidal cell synapse [36]. Together these results indicate that Neto1 specifically modulates not only the kinetics but also the amplitude of KAR-EPSCs.

Localization of kainate receptors is independent of Neto1 and its PDZ-binding

Neto1 contains a canonical binding motif (-TTRV) of the class I PDZ domain at its C-terminus (Supplementary Fig. 1a). Although the surface expression of the KAR/Neto complex is mediated by KARs, the mechanism for synaptic localization of KARs remains uncertain. The significant changes in KAR-mediated transmission in the Neto1-knockout mouse (Fig. 5a) could be due to the loss of KARs at synapses or changes in receptor function. To address this issue, we evaluated protein distribution and synaptic expression in wild-type and Neto1-knockout mice.

GluK2/3 localization was detected at the CA3 *s. lucidum* using anti-GluK2/3 antibody, where no obvious difference was observed in the distribution of GluK2/3 in the hippocampus between wild-type and Neto1-knockout mice (Fig. 6a). High-magnification confocal images showed a loss of the GluK2/3 signal in the hippocampus *s. lucidum* in GluK2-knockout mice, with no obvious difference in Neto1-knockout mice (Fig. 6a,b). Similarly, we did not detect any significant difference in GluK5 distribution in Neto1-knockout mice, suggesting that Neto1 acts independently from GluK5 (Supplementary Fig. 5). In addition, we measured protein expression in the PSD fraction. Mouse hippocampi were dissected and fractionated biochemically into each organelle, and Neto1 was strongly detected in the PSD fraction (Fig. 6c). Using the same method, we found no difference in the expression levels of ionotropic glutamate receptors and synaptic proteins in the PSD from hippocampi from hetero- and homozygous Neto1-knockout mice (Fig. 6d). Finally, we compared expression of GluN2A and B in hippocampi from wild-type and Neto1-knockout mice, and did not detect any difference in protein expression at the PSD (Fig. 6d). From these results, we conclude that Neto1 regulates KAR-mediated transmission through modulation of channel properties, but not synaptic localization.

Neto1 influences kainate receptor-driven charge transfer and spike fidelity

Recent evidence has demonstrated a role for synaptic KARs in mediating spike transmission between granule cells of the dentate gyrus and CA3 pyramidal cells[18]. In light of these findings we sought to determine how Neto1 may contribute to this process. We found that the charge transfer generated by brief bursts (5 pulses) of presynaptic stimulation at 3, 10, and 30 Hz while recording CA3 neurons in the whole-cell voltage clamp configuration (Fig. 7a) was reduced in Neto1-knockout animals relative to wild-type littermates (Fig. 7b) (WT: 3 Hz 2.01 ± 0.19; 10 Hz 3.99 ± 0.56; 30 Hz 4.44 ± 0.80, 7 cells, 3 animals. KO: 3 Hz 0.52 ± 0.12, p=0.0018; 10 Hz 1.33 ± 0.12, p= 0.0078; 30 Hz 1.72 ± 0.35 p= 0.0321, 8 cells, 4 animals). In line with our previous results indicating a postsynaptic locus of Neto1, the ratio

of the amplitude of the 5th pulse to the 1st pulse was unchanged between these experimental groups strongly suggesting no change in basal presynaptic function in Neto1 knockout mice (Fig. 7c). Consistent with this observation, paired-pulse facilitation was normal in Neto1-knockout animals (Supplementary Fig. 6a,b). Additionally, we tested whether Neto 1 deletion could affect presynaptically expressed mossy fiber LTP, but found no significant difference in the magnitude of LTP between Neto 1-knockout and wild-type mice (Supplementary Fig. 6c,d). Finally, we explored the role of Neto1 in spike generation through summation of KAR-mediated excitatory postsynaptic potentials (EPSPs). Spikes were generated in CA3 pyramidal cells by a burst of presynaptic stimulation (30Hz) such that a spike was elicited after the 4th pulse 50% of the time, as a strategy to normalize the varying input resistances across cells. Under these conditions we observed a significant decrease in the probability of a spike occurring after the 5th pulse in Neto1-knockout animals compared to wild-type littermate controls (WT: 83.4 ± 6.4, 7 cells, 3 animals; KO: 52.1 ± 5.9, 7 cells, 3 animals, p= 0.0025) (Fig. 7d,e). Similar results were obtained under more physiological recording conditions, namely, without pharmacologically isolating KAR-mediated EPSPs (WT: 79.7 ± 5%, 6 cells, 3 animals; KO: 63.3 ± 3.8%, 6 cells, 3 animals, p=0.0025)(Fig. 7f). Additionally, analyzing the coefficient of variation in latency of spikes to the stimulation pulse (jitter), demonstrated that spike jitter was significantly higher in Neto1-knockout mice than in their wild-type littermates (WT 0.072 ± 0.005, 3 cells, 3 animals; KO 0.64 ± 0.17, 3 cells, 3 animals, p= 0.00013). As shown in Supplementary Fig. 7, Neto 1 deletion did not affect intrinsic properties of CA3 pyramidal cells. Together, these results suggest that the efficacy of postsynaptic KARs in mediating spike transmission at the mf-CA3 synapse can be regulated by Neto1.

Discussion

In this study, we report that KAR slow kinetics and high affinity binding in the brain, presumably the two most distinct properties of native KARs, are determined by the auxiliary subunit Neto1. This KAR auxiliary subunit augments the agonist binding affinity and off-kinetics of KARs. Additionally, Neto1 controls the decay kinetics and amplitude of KAR-EPSCs by modulating the channel properties, rather than KAR synaptic expression. As a result of this modification, the postsynaptic KAR/Neto1 complex can regulate KAR-EPSC spike generation, indicating a potential role for this complex in modulating neural circuit function.

A perennial question in the field has been how the distinct distribution of high-affinity KAR in the brain is defined. Strong [3H]kainate binding signals can be observed in the hippocampal *s. lucidum*[6]. However, this experimental approach alone cannot distinguish between binding to pre or postsynaptic KARs. Here, we found that disruption of Neto1 in CA3 pyramidal cells, as indicated by our anatomical, biochemical and electrophysiological evidence, diminished most of the [3H]kainate binding (Fig. 3), consistent with functional evidence that the KARs in the *s. lucidum* are predominantly localized postsynaptically[41]. However, we still detected 50% residual high-affinity KARs in biochemical binding experiments. The residual binding could be the result of KARs associated with the Neto1 homologue Neto2, which is also expressed in CA3 pyramidal cells albeit at lower levels (Fig. 1a)[38]. Alternatively, this binding could reflect presynaptic KARs that lack Netos. To

distinguish between these possibilities, an analysis of the Neto1/ Neto2 double knockout will be required.

Several KAR binding proteins have been reported to support synaptic localization of KARs, and most are PDZ binding proteins that recognize the GluK2 PDZ binding motif[31, 32, 34, 35, 42]. Neto1 possesses a typical class 1 PDZ binding domain (-TTRV) at its C-terminus. Indeed, a PDZ dependent interaction of Neto1 with PSD-95 was previously reported[36], although we could not confirm this interaction *in vivo* (Fig. 1b). Our findings show that loss of Neto1 impaired KAR-mediated synaptic transmission without obvious changes in the distribution of KARs. We therefore conclude that the KAR itself, but not Neto1, possesses the signal for its synaptic localization. Consistent with this possibility, a reduction in synaptic KAR distribution has recently been reported in GluK4/5 double knockouts, indicating that the GluK4/5 subunits partly determine the synaptic localization of the KAR complex[43]. We also found that GluK2/3 binds preferentially to Neto2 in the cerebral cortex, suggesting a robust interaction between GluK2/3 and Neto2 (Fig. 1b). It is worth noting that the GluK2/3 antibody we used likely recognizes one of three GluK2/3 splicing isoforms[44]. An alternative scenario is that Neto1 and Neto2 might interact preferentially with specific KAR splicing isoforms.

Another query of longstanding contention has been that the slow decay kinetics of native KAR-EPSCs are significantly different from the fast kinetics of recombinant KARs expressed in heterologous cells. The underlying explanation for this discrepancy has been elusive, while various mechanisms have been proposed[1, 2, 44, 45]. For example, KARs could be located extrasynaptically and be activated by glutamate spillover. However, this possibility was discarded early on given that reducing glutamate diffusion and/or antagonizing glutamate reuptake failed to alter the kinetics and amplitude of KAR-EPSCs[7, 10, 14]. Another possibility is that the presence of GluK5 could confer slow gating properties to native KARs. However, as GluK5 slows down glutamate-induced currents of recombinant GluK2/5 in heterologous cells[46], KAR-EPSCs are slightly faster in GluK5 knockout mice[47]. Importantly, our results reveal that the decay kinetics of KAR-EPSCs at the mf-CA3 synapse is significantly faster in Neto1-knockout mice (Fig. 5a) strongly suggesting that Neto1 is a major determinant in generating the characteristically slow decay kinetics of native KAR-EPSCs.

A recent study has reported that Neto1 is an NMDAR-interacting protein[36]. According to this study, Neto1 co-immunoprecipitates with NMDARs and also regulates NMDAR-mediated transmission and NMDAR-dependent LTP in the CA1 region of the hippocampus. In contrast to these findings, we were unable to demonstrate any biochemical interaction between Neto1 and the NMDAR, or change in NMDAR-mediated transmission at synapses impinging on CA3 pyramidal cells where Neto1 is strongly expressed[36, 38, 48] and the current study. This apparent discrepancy might be caused by differences in the genetic background of the two Neto1 KO lines. The Neto1 KO line in the present study was generated using VGB6 ES cell lines derived from C57BL/6NT$_{AC}$ and backcrossed with C57BL/6J at least 6 times, whereas the other Neto1 KO line[36] was generated using the R1 ES cells (129X1/SvJ) and backcrossed with C57BL/6J, presumably rendering a 129/BL6 hybrid genetic background. Notably, Neto1 mRNA is strongly expressed in hippocampal

CA3 pyramidal cells and CA1 interneurons[36, 38], a pattern more consistent with the functional expression of KARs, and our findings that Neto1 is an auxiliary subunit specific to KARs.

In addition to mediating synaptic transmission (e.g. KAR-EPSCs), KARs can also regulate transmitter release[4]. However, we found no functional or anatomical evidence that Neto1 regulates presynaptic KAR function. We have shown that the capability of KAR-EPSCs to elicit action potentials from CA3 pyramidal cells in a robust and temporally precise manner is diminished in the Neto1-knockout. These findings, when viewed in the context of the function of the hippocampal tri-synaptic circuit, could be relevant to specific types of hippocampal memory function.

Methods

Antibodies

The following antibodies were used: rabbit polyclonal antibodies to GluA2/3, GluK2/3, GluK5 (Millipore), Neuropilin 1 (Calbiochem) and Beta-tubulin (Sigma); mouse monoclonal antibodies to GluN1, GluN2A and GluN2B (BD Biosciences), PSD-95 (ABR), synaptophysin (Sigma) and Actin (Chemicon). Rabbit polyclonal antibodies to Neto2 were described before[33] and isoform specific antibodies against Neto1 and Neto2 were generated with GST- fusion proteins encoding different c-terminal sequences (see Supplementary Fig. 1). Antisera were affinity-purified on agarose columns containing His-Neto1/2 fusion proteins. In addition, guinea pig polyclonal antibody against Neto1 was generated for immunohistochemistry.

Neto1-knockout mice

We obtained the Neto1 targeted ES cells and mice from a trans-NIH initiative, The Knockout Mouse Project (KOMP, www.komp.org). We maintained Neto1-knockout mice by crossing heterozygous males and females. Animal handling and use followed a protocol approved by the institutional Animal Care and Use Committee both at Yale University and Albert Einstein College of Medicine, in accordance with National Institutes of Health guidelines.

Biochemical analysis of protein expression and interactions

Total protein expression, PSD fraction and co-immunoprecipitation were performed as described[33]. Surface expression of glutamate receptors was quantified as described[40]. Briefly, hippocampal acute brain slices were prepared from 4-week-old mice and labeled for 30 min at 4°C with 1.5mg/ml sulfo-NHS-SS biotin. Crude membrane fractions were prepared and biotinylated proteins were precipitated with neutravidin-agarose and analyzed by western blot.

[^{3}H]kainate binding

Hippocampi were dissected from 4-week-old mice, homogenized in 50 mM Tris-citrate pH7.0 and centrifuged at 100,000 × g for 30min. This step was repeated three times and membranes were resuspended in 50 mM Tris-citrate pH7.0. To measure [^{3}H]kainate binding

from HEK-cells transfected with GluK2 with- or without Neto1, cells were harvested 48 hour later and cell membranes were prepared as above. Cell suspension was incubated with [^{3}H]kainate (Perkin Elmer) for 1 h on ice, followed by filtration with GF/B Glass Microfibre Filter (Whatman International, UK) that were presoaked in 0.1% Polyethyleneimine. After washing twice, the filter was incubated in scintillation fluid (American Bioanalytical, MA) for 1 h at room temperature and analyzed in a scintillation counter. Specific binding was defined as signal decrease in the presence of 1 mM unlabeled KA, and all samples were performed in triplicate. For GluK2-specific binding, the signal from membranes from GluK2-knockout mice was subtracted. To ensure protein levels were similar protein expression in each sample was analyzed by western blot. Data was fitted to the Hill equation.

For [^{3}H]kainate binding in hippocampal sections, fresh brains were shock-frozen in dry ice. Coronal brain sections (20 μm) were prepared, incubated for 1 h at 4°C in 50 mM Tris-citrate pH7.0, washed for 10 min at room temperature in the same buffer and incubated in 50 nM [^{3}H]kainate (37Ci/mmol, PerkinElmer, MA) for 45min on ice. Sections were then rinsed three times for 10 s with ice-cold buffer and rapidly frozen. After lyophilization, sections were dipped in emulsion (Amersham, UK), dried and stored at 4°C for in darkness seven weeks. Autoradiograms were then developed and analyzed by light microscopy.

Histochemistry

Under deep pentobarbital anesthesia, mice were perfused transcardially with 4% paraformaldehyde in 0.1 M sodium phosphate buffer (PB; pH 7.2) for immunohistochemistry. Brains to be compared simultaneously were embedded in single paraffin blocks, and sections (4 μm in thickness) were made with a sliding microtome (SM1000R; Leica). Microslicer sections were also used for immunofluorescence (40 μm; VT1000S, Leica). All immunohistochemical incubations were done at room temperature. For light microscopic immunohistochemistry, sections were first subjected to pepsin pretreatment for antigen exposure, i.e., incubation in 1 mg/ml of pepsin (DAKO) in 0.2 N HCl for 10 min at 37°C. Then sections were incubated successively with 10% normal goat serum for 20 min, primary antibodies (1 μg/ml) overnight, biotinylated secondary antibodies for 2 h and avidin-biotin-peroxidase complex for 1 h, using a Histofine SAB-PO(R) kit (Nichirei Corp.). Immunoreaction was visualized using the tyramide signal amplification kit (PerkinElmer).

Mice were perfused with 4% PFA and sections (40 μm) were cut at room temperature. The sections were processed to immunofluorescence staining with various antibodies and X-gal staining to monitor beta-galactosidase activity. For immunofluorescense staining, brain sections were treated with pepsin, followed by permeabilization with 0.2% Triton X-100. After blocking with 3% goat serum, sections were incubated in primary antibody, followed by fluorescent-conjugated secondary antibodies and mounted on glass slides. Fluorescent images were captured by confocal microscopy (LSM510 meta, Zeiss; FV1000, Olympus). For X-gal staining, sections were washed with PBS containing 2 mM $MgCl_2$ and incubated for 4-12 h in X-gal reaction buffer, containing 0.25 mg/ml X-gal in PBS with 35 mM

K_4[Fe(CN)6], 35 mM K_3[Fe(CN)$_6$], 0.02% NP-40 and 0.01% Na-deoxycholate. Sections were then washed with PBS, mounted and bright-field images were taken.

Analysis of channel kinetics

GluK2 and Neto1 were cloned into pCAGGS vector containing IRES-GFP or mCherry, respectively, and co-transfected with GluK5 into tsA201 cells, using Lipofectamine2000 (Invitrogen). Transfection ratio of Gluk2, GluK5 and Neto1 was 1:3:10, and expression was confirmed by western blotting. Recordings from outside-out patches were performed at room temperature at a holding potential of -70 mV. The external solution was (in mM): 140 NaCl, 2.5 KCl, 2.5 $CaCl_2$, 2.7 $MgCl_2$, 1.3 $MgSO_4$, 10 glucose, and 10 HEPES (pH 7.4). Patch pipettes (open tip resistance 2 to 3 MΩ) were filled with a solution containing (in mM): 145 $CsMeSO_4$, 20 TEA-Cl, 5 Mg-ATP, 0.2 Na-GTP, 5 EGTA, and 5 HEPES (pH 7.25). The size of the peak currents was 0.5 to 2 nA (60-70% series resistance compensation). Kainate (1mM) in extracellular solution was applied with theta glass pipettes mounted on a piezoelectric bimorph. Agonist-evoked currents were analog low-pass filtered at 3 kHz, sampled at 25 kHz, and analyzed with Igor software [49]. The results were fitted with an equation consisting of two Hodgkin-Huxley components [33].

Synaptic physiology

Hippocampal and cerebellar slices were prepared from mice (17–30 days old). After animals were deeply anesthetized with isoflurane, they were decapitated and the brain rapidly removed into chilled cutting solution consisting of (in mM) 215 sucrose, 2.5 KCl, 20 glucose, 26 $NaHCO_3$, 1.6 NaH_2PO_4, 1 $CaCl_2$, 4 $MgCl_2$, and 4 $MgSO_4$. Hippocampi or cerebellum were dissected out and cut into 400 mm thick (transverse or sagittal respectively) sections on a Leica VT 1200s vibrating microslicer (Leica, Ltd., Germany). The cutting solution was slowly exchanged with artificial cerebrospinal fluid (ACSF) containing (in mM) 124 NaCl, 2.5 KCl, 10 glucose, 26 $NaHCO_3$, 1.0 NaH_2PO_4, 2.5 $CaCl_2$, and 1.3 $MgCl_2$. Both cutting and ACSF solutions were saturated with 95% O_2 and 5% CO_2 (pH 7.4). The slices were incubated at room temperature for at least 1.5 hr before recording, and then were transferred as needed to a submersion-type recording chamber perfused with ACSF at 2 ml/min.

Whole-cell recordings of CA3 pyramidal cells were obtained using standard techniques. To maximize cell health and recording stability, cells deep below the surface of the slice were recorded semi-“blind”. CA1 interneuron and cerebellar Purkinje cell recordings were obtained by visualized patch technique. The recording pipette resistance ranged between 3 and 4 MΩ. Series resistance (6–15MΩ) and input resistance were monitored throughout each voltage-clamp recording with 80 ms, -4mV steps. Recordings with >10% change in series resistance were systematically excluded. The recording pipette solution for voltage-clamp recordings was (in mM) 123 cesium gluconate, 1 $CaCl_2$, 10 EGTA, 10 HEPES, 10 glucose, pH 7.3 290-295 mOsm. The pipette solution for current-clamp recordings contained (in mM) 135 K-gluconate, 5 KCl, 1 $CaCl_2$, 5 EGTA-Na, 10 HEPES, 10 glucose, 5 MgATP, and 0.4 Na_3GTP. Resting potential ranged from -69 to -58 mV. Maximal recording time after dissection was 6 hr. Recording temperature was set to 25.0 ± 0.1 C° using a TC-344B dual-channel temperature controller (Warner Instruments, Inc, Hamden, CT, USA).

Synaptic afferents were activated by monopolar stimulation delivered via a patch-type pipette broken to a tip diameter of ∼10 μm and filled with external saline. This stimulating electrode was placed in the dentate gyrus cell body layer to activate mfs and in the CA3 *s. radiatum* to activate ac fibers. The baseline stimulation rate was 0.1 Hz for most experiments, except those shown in Fig. 7 where a rate of 0.03 Hz inter-burst stimulation was used and for mossy fiber LTP where baseline stimulation rate was 0.05 Hz. To assess the contribution of mf-CA3 transmission, 1 μM DCG-IV, a group II mGluR agonist that selectively blocks mossy fiber synaptic transmission, was applied at the end of every experiment, and the data were accepted only if synaptic responses were reduced by more than 90%. The synaptic response remaining in DCG-IV was then subtracted from all previous responses before further analysis to isolate mf-specific synaptic activity. KAR-EPSC were monitored in the presence of the selective AMPAR antagonist GYKI 53655 (30 μM) and cells were voltage-clamped to -60 mV or +30mV. KAR-mediated mf-CA3 EPSCs/EPSPs were evoked by single or brief repetitive stimulation in the dentate gyrus. Unless otherwise noted, NMDAR-EPSCs were monitored in 10 μM NBQX, 100 μM picrotoxin, and 3 μM CGP55845 while voltage-clamping to +30mV. Given the variability and potential polysynaptic contamination of AMPAR mediated EPSCs at mf-CA3 synapses [41], AMPAR-mediated transmission was evaluated by activating ac-CA3 synapses (Vh = -60 mV) in the presence of 50 μM d-APV, 100 μM picrotoxin, and 3 μM CGP 55845 (Fig. 4). Analysis of decay kinetics was carried out by fitting trace averages with a single exponential. Rise time values were assessed by measuring the time course from 10-90% of the total response amplitude. To measure AMPAR/NMDAR ratios, EPSCs were evoked by stimulating AC fibers. Cells were recorded at -60 mV to acquire AMPAR-EPSCs and then held at +30 mV in the presence of 10 μM NBQX to acquire NMDA-EPSCs. Normalized charge transfer values were calculated by normalizing trace averages to the amplitude of the 1 pulse in the train and integrating the resultant area under the curve. To assess synaptic facilitation with a 5–stimuli burst, the Pulse 5/Pulse 1 amplitude ratio was used (Fig 6a,c). The amplitude of the 5^{th} pulse was measured by digitally subtracting the first four pulses. Mossy fiber LTP was induced after at least 15 min of stable baseline by tetanic stimulation including 2 trains (20-s interval) each containing 125 pulses at 25Hz in presence of 50 μM D-APV. LTP magnitude was quantified by averaging normalized mossy fiber responses for 10 minute periods before and 30 min after tetanic stimulation. Spike jitter was calculated by taking the raw latency values and dividing the standard deviation by the mean to yield the resultant coefficient of variation. Averaged traces include at least 10 successive synaptic responses. All experiments were executed with a MultiClamp 700B (Axon Instruments Inc./Molecular Devices, Union City, CA, USA). Electrophysiological data were digitized (3–5 kHz) and analyzed on-line using custom-made software for IgorPro (Wavemetrics Inc., Lake Oswego, OR, USA). NBQX, D-APV, picrotoxin, CGP 55845, DCG-IV, GYKI 53655 (custom ordered), MK-801, were obtained from Tocris-Cookson Inc. (Ellisville, MO, USA). All other chemicals were purchased from Sigma-Aldrich (St. Louis, MO, USA).

Statistical analysis

All data are given as mean ± s.e.m. Statistical significance between means was calculated using unpaired Student's t test. In all figures, error bars indicate ± s.e.m., and averaged traces include 15–30 consecutive individual responses.

Supplementary Material

Refer to Web version on PubMed Central for supplementary material.

Acknowledgments

The authors thank members of the Tomita lab and Castillo lab for helpful discussions. We thank Dr. Michelle T.W. Ho for technical advice on slice preparation, Mr. Gerard Somers for maintaining mouse colonies, Dr. S.F. Heinemann (Salk Institute) for generating GluK2 KO mice and the KOMP for creating Neto1 KO mice. S.T. is supported by NIH/NIMH R01 MH085080. P.E.C is supported by NIH/NIMH R01 MH081935. C.S. is supported by a Boehringer-Ingelheim PhD fellowship. M.W. is supported by Grants-in-Aid for Scientific Research (19100005) provided by the Ministry of Education, Culture, Sports, Science and Technology of Japan.

References

1. Traynelis SF, et al. Glutamate receptor ion channels: structure, regulation, and function. Pharmacol Rev. 2010; 62:405–496. [PubMed: 20716669]
2. Lerma J. Kainate receptor physiology. Curr Opin Pharmacol. 2006; 6:89–97. [PubMed: 16361114]
3. Contractor A, Mulle C, Swanson GT. Kainate receptors coming of age: milestones of two decades of research. Trends Neurosci. 2011; 34:154–163. [PubMed: 21256604]
4. Pinheiro PS, Mulle C. Presynaptic glutamate receptors: physiological functions and mechanisms of action. Nat Rev Neurosci. 2008; 9:423–436. [PubMed: 18464791]
5. Jane DE, Lodge D, Collingridge GL. Kainate receptors: pharmacology, function and therapeutic potential. Neuropharmacology. 2009; 56:90–113. [PubMed: 18793656]
6. Foster AC, Mena EE, Monaghan DT, Cotman CW. Synaptic localization of kainic acid binding sites. Nature. 1981; 289:73–75. [PubMed: 6256647]
7. Castillo PE, Malenka RC, Nicoll RA. Kainate receptors mediate a slow postsynaptic current in hippocampal CA3 neurons. Nature. 1997; 388:182–186. [PubMed: 9217159]
8. Vignes M, Collingridge GL. The synaptic activation of kainate receptors. Nature. 1997; 388:179–182. [PubMed: 9217158]
9. Kidd FL, Isaac JT. Developmental and activity-dependent regulation of kainate receptors at thalamocortical synapses. Nature. 1999; 400:569–573. [PubMed: 10448859]
10. Kidd FL, Isaac JT. Kinetics and activation of postsynaptic kainate receptors at thalamocortical synapses: role of glutamate clearance. J Neurophysiol. 2001; 86:1139–1148. [PubMed: 11535664]
11. Wu LJ, Zhao MG, Toyoda H, Ko SW, Zhuo M. Kainate receptor-mediated synaptic transmission in the adult anterior cingulate cortex. J Neurophysiol. 2005; 94:1805–1813. [PubMed: 15928066]
12. Li H, Rogawski MA. GluR5 kainate receptor mediated synaptic transmission in rat basolateral amygdala in vitro. Neuropharmacology. 1998; 37:1279–1286. [PubMed: 9849665]
13. Li P, et al. Kainate-receptor-mediated sensory synaptic transmission in mammalian spinal cord. Nature. 1999; 397:161–164. [PubMed: 9923678]
14. Bureau I, Dieudonne S, Coussen F, Mulle C. Kainate receptor-mediated synaptic currents in cerebellar Golgi cells are not shaped by diffusion of glutamate. Proc Natl Acad Sci U S A. 2000; 97:6838–6843. [PubMed: 10841579]
15. Frerking M, Malenka RC, Nicoll RA. Synaptic activation of kainate receptors on hippocampal interneurons. Nat Neurosci. 1998; 1:479–486. [PubMed: 10196545]
16. Wondolowski J, Frerking M. Subunit-dependent postsynaptic expression of kainate receptors on hippocampal interneurons in area CA1. J Neurosci. 2009; 29:563–574. [PubMed: 19144856]
17. Frerking M, Ohliger-Frerking P. AMPA receptors and kainate receptors encode different features of afferent activity. J Neurosci. 2002; 22:7434–7443. [PubMed: 12196565]
18. Sachidhanandam S, Blanchet C, Jeantet Y, Cho YH, Mulle C. Kainate receptors act as conditional amplifiers of spike transmission at hippocampal mossy fiber synapses. J Neurosci. 2009; 29:5000–5008. [PubMed: 19369569]
19. Cunningham MO, et al. Neuronal metabolism governs cortical network response state. Proc Natl Acad Sci U S A. 2006; 103:5597–5601. [PubMed: 16565217]

20. Paternain A, Rodríguez-Moreno A, Villarroel A, Lerma J. Activation and desensitization properties of native and recombinant kainate receptors. Neuropharmacology. 1998; 37:1249–1259. [PubMed: 9849662]
21. Herb A, et al. The KA-2 subunit of excitatory amino acid receptors shows widespread expression in brain and forms ion channels with distantly related subunits. Neuron. 1992; 8:775–785. [PubMed: 1373632]
22. Heckmann M, Bufler J, Franke C, Dudel J. Kinetics of homomeric GluR6 glutamate receptor channels. Biophys J. 1996; 71:1743–1750. [PubMed: 8889151]
23. Schiffer HH, Swanson GT, Heinemann SF. Rat GluR7 and a carboxy-terminal splice variant, GluR7b, are functional kainate receptor subunits with a low sensitivity to glutamate. Neuron. 1997; 19:1141–1146. [PubMed: 9390526]
24. Traynelis SF, Wahl P. Control of rat GluR6 glutamate receptor open probability by protein kinase A and calcineurin. J Physiol. 1997; 503:513–531. [PubMed: 9379408]
25. Swanson GT, Heinemann SF. Heterogeneity of homomeric GluR5 kainate receptor desensitization expressed in HEK293 cells. J Physiol. 1998; 513:639–646. [PubMed: 9824706]
26. Cui C, Mayer ML. Heteromeric kainate receptors formed by the coassembly of GluR5, GluR6, and GluR7. J Neurosci. 1999; 19:8281–8291. [PubMed: 10493729]
27. Mott DD, Rojas A, Fisher JL, Dingledine RJ, Benveniste M. Subunit-specific desensitization of heteromeric kainate receptors. J Physiol. 2010; 588:683–700. [PubMed: 20026616]
28. Erreger K, Chen PE, Wyllie DJ, Traynelis SF. Glutamate receptor gating. Crit Rev Neurobiol. 2004; 16:187–224. [PubMed: 15701057]
29. Swanson GT, et al. Differential activation of individual subunits in heteromeric kainate receptors. Neuron. 2002; 34:589–598. [PubMed: 12062042]
30. Bowie D, Garcia EP, Marshall J, Traynelis SF, Lange GD. Allosteric regulation and spatial distribution of kainate receptors bound to ancillary proteins. J Physiol. 2003; 547:373–385. [PubMed: 12562952]
31. Garcia EP, et al. SAP90 binds and clusters kainate receptors causing incomplete desensitization. Neuron. 1998; 21:727–739. [PubMed: 9808460]
32. Laezza F, et al. KRIP6: a novel BTB/kelch protein regulating function of kainate receptors. Mol Cell Neurosci. 2007; 34:539–550. [PubMed: 17254796]
33. Zhang W, et al. A transmembrane accessory subunit that modulates kainate-type glutamate receptors. Neuron. 2009; 61:385–396. [PubMed: 19217376]
34. Coussen F, et al. Recruitment of the kainate receptor subunit glutamate receptor 6 by cadherin/catenin complexes. J Neurosci. 2002; 22:6426–6436. [PubMed: 12151522]
35. Hirbec H, et al. Rapid and differential regulation of AMPA and kainate receptors at hippocampal mossy fibre synapses by PICK1 and GRIP. Neuron. 2003; 37:625–638. [PubMed: 12597860]
36. Ng D, et al. Neto1 is a novel CUB-domain NMDA receptor-interacting protein required for synaptic plasticity and learning. PLoS Biol. 2009; 7:e41. [PubMed: 19243221]
37. Mulle C, et al. Altered synaptic physiology and reduced susceptibility to kainate-induced seizures in GluR6-deficient mice. Nature. 1998; 392:601–605. [PubMed: 9580260]
38. Michishita M, et al. Expression of Btcl2, a novel member of Btcl gene family, during development of the central nervous system. Brain Res Dev Brain Res. 2004; 153:135–142. [PubMed: 15464227]
39. Berger M, Ben-Ari Y. Autoradiographic visualization of [3H]kainic acid receptor subtypes in the rat hippocampus. Neurosci Lett. 1983; 39:237–242. [PubMed: 6314197]
40. Tomita S, Fukata M, Nicoll RA, Bredt DS. Dynamic interaction of stargazin-like TARPs with cycling AMPA receptors at synapses. Science. 2004; 303:1508–1511. [PubMed: 15001777]
41. Kwon HB, Castillo PE. Role of glutamate autoreceptors at hippocampal mossy fiber synapses. Neuron. 2008; 60:1082–1094. [PubMed: 19109913]
42. Salinas GD, et al. Actinfilin is a Cul3 substrate adaptor, linking GluR6 kainate receptor subunits to the ubiquitin-proteasome pathway. J Biol Chem. 2006; 281:40164–40173. [PubMed: 17062563]
43. Fernandes HB, et al. High-affinity kainate receptor subunits are necessary for ionotropic but not metabotropic signaling. Neuron. 2009; 63:818–829. [PubMed: 19778510]

44. Pinheiro P, Mulle C. Kainate receptors. Cell Tissue Res. 2006; 326:457–482. [PubMed: 16847640]
45. Lerma J. Roles and rules of kainate receptors in synaptic transmission. Nat Rev Neurosci. 2003; 4:481–495. [PubMed: 12778120]
46. Barberis A, Sachidhanandam S, Mulle C. GluR6/KA2 kainate receptors mediate slow-deactivating currents. J Neurosci. 2008; 28:6402–6406. [PubMed: 18562611]
47. Contractor A, et al. Loss of kainate receptor-mediated heterosynaptic facilitation of mossy-fiber synapses in KA2-/- mice. J Neurosci. 2003; 23:422–429. [PubMed: 12533602]
48. Michishita M, et al. A novel gene, Btcl1, encoding CUB and LDLa domains is expressed in restricted areas of mouse brain. Biochem Biophys Res Commun. 2003; 306:680–686. [PubMed: 12810072]
49. Tomita S, et al. Stargazin modulates AMPA receptor gating and trafficking by distinct domains. Nature. 2005; 435:1052–1058. [PubMed: 15858532]

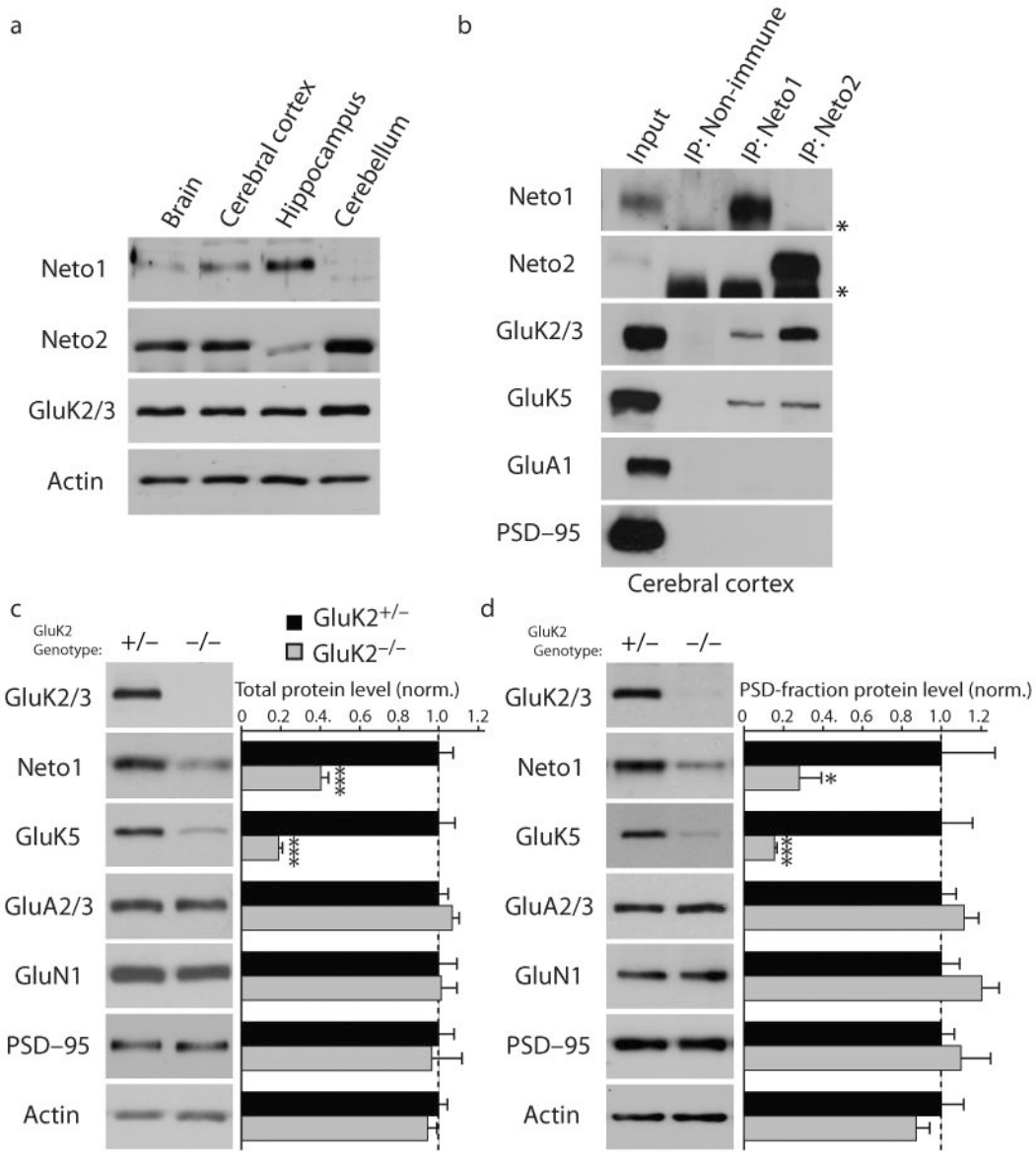

Figure 1.

Hippocampus-abundant Neto1 interacts with kainate receptors *in vivo*. (**a**) Distinct expression of Neto1 and Neto2 in the brain. Neto1 expressed strongly in hippocampus, whereas Neto2 expressed in all brain regions except hippocampus. (**b**) Neto1 and Neto2 co-immunoprecipitated with GluK2/3 and GluK5, but not with GluA1 or PSD95, from rat brain lysate. Asterisk indicates Ig heavy chain. (**c**) Total protein levels of Neto1 and GluK5 were reduced in hippocampus from GluK2 knockout (−/−) compared to heterozygous (+/−), demonstrating a genetic interaction between GluK2 and Neto1 together with GluK5. Signal intensities were measured and normalized by those from Neto1 heterozygous (n = 4). (**d**) To compare protein expression at the postsynaptic density (PSD), PSDs were fractionated from hippocampi of the indicated genotypes (n = 4 each). Data are given as mean ± s.e.m.; * $P <$ 0.05, *** $P <$ 0.005.

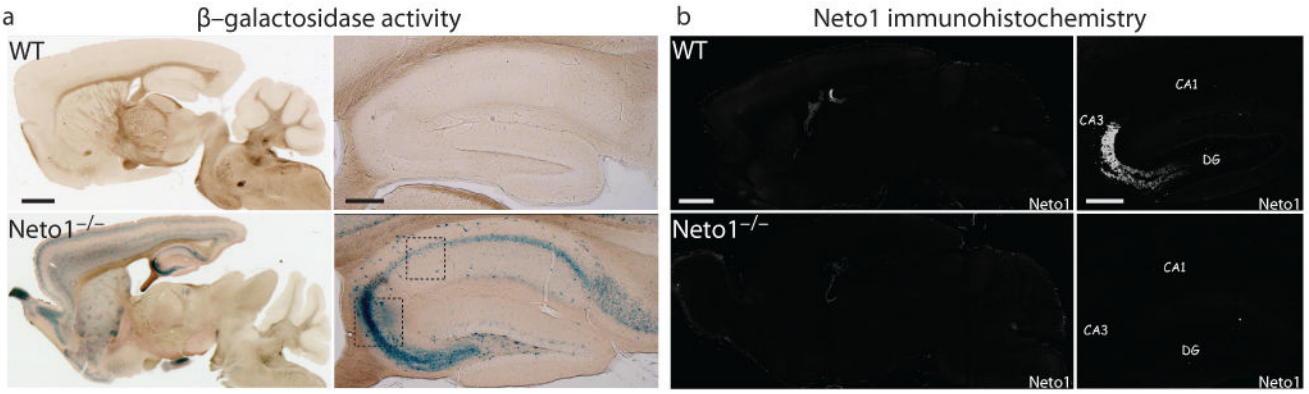

Figure 2.

Neto 1 is highly expressed in the hippocampus CA3 pyramidal neurons and localizes at *s. lucidum*. (**a**) Endogenous Neto1 promoter activity was monitored by beta-galactosidase activity in the knockout (−/−), in which the Neto1 gene was replaced with beta-galactosidase. Strong beta-galactosidase activity was observed in the hippocampus CA3 pyramidal cells, whereas weak activity was observed in the hippocampus CA1 interneurons, cerebral cortex, and striatum. Boxes represent regions where the recordings were performed in Fig. 4a-c. (**b**) Localization of Neto1 protein shown by immunohistochemistry with an anti-Neto1 antibody. Neto1 localized strongly at the hippocampus *s. lucidum*, where mossy fiber and CA3 pyramidal cells form synapses, in the wild type (WT), but not in the Neto1-knockout (−/−). Scale bars: Left panel, 1mm; Right panel, 200 μm.

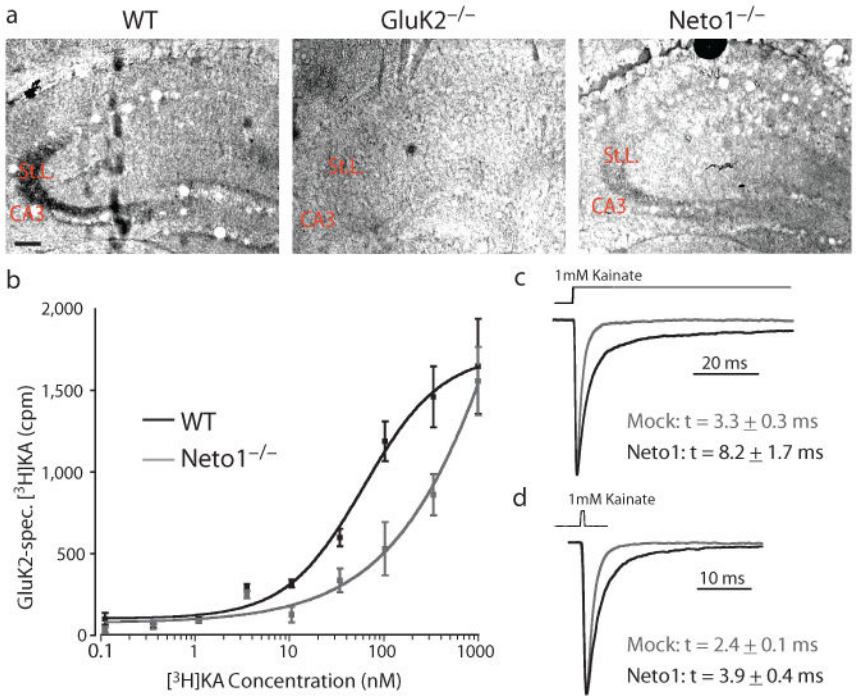

Figure 3.

Distinct distribution of high-affinity kainate receptors is determined by Neto1 postsynaptically. (**a**) Kainate binding in coronal hippocampal sections were visualized using an autoradiographical technique with [^{3}H]kainate (50 nM). A strong [^{3}H]kainate signal was observed in the *s. lucidum* (St. L.) in the wild type, but not in the GluK2 knockout (−/−). On the other hand, the [^{3}H]kainate signal was reduced in Neto1-knockout mice (−/−). Scale bar: 100 μm. (**b**) Binding of carious concentration of [^{3}H]kainate to hippocampal membranes was measured. The binding curve was shifted to the right in the Neto1-knockout. (**c,d**) Comparison of channel properties in transfected heterologous cells using a piezo-driven fast-perfusion system in outside-out patches. GluK2 and GluK5 were co-expressed with empty plasmid (Mock) or Neto1 in tsA201 cells. Representative response to sustained 1mM kainate application (**c**) and a 1-ms pulse (**d**). (**c**) Co-expression of Neto1 slowed desensitization and increased the ratio of steady-state and peak currents of GluK2/5 heteromeric channels (n=7-12). (**d**) Neto1 slowed deactivation of GluK2/5 (n=7-9). Upper traces in **c** and **d** indicate the open-tip potential to confirm rate of solution exchange. Data are given as mean ± s.e.m.; * $P < 0.05$, ** $P < 0.01$.

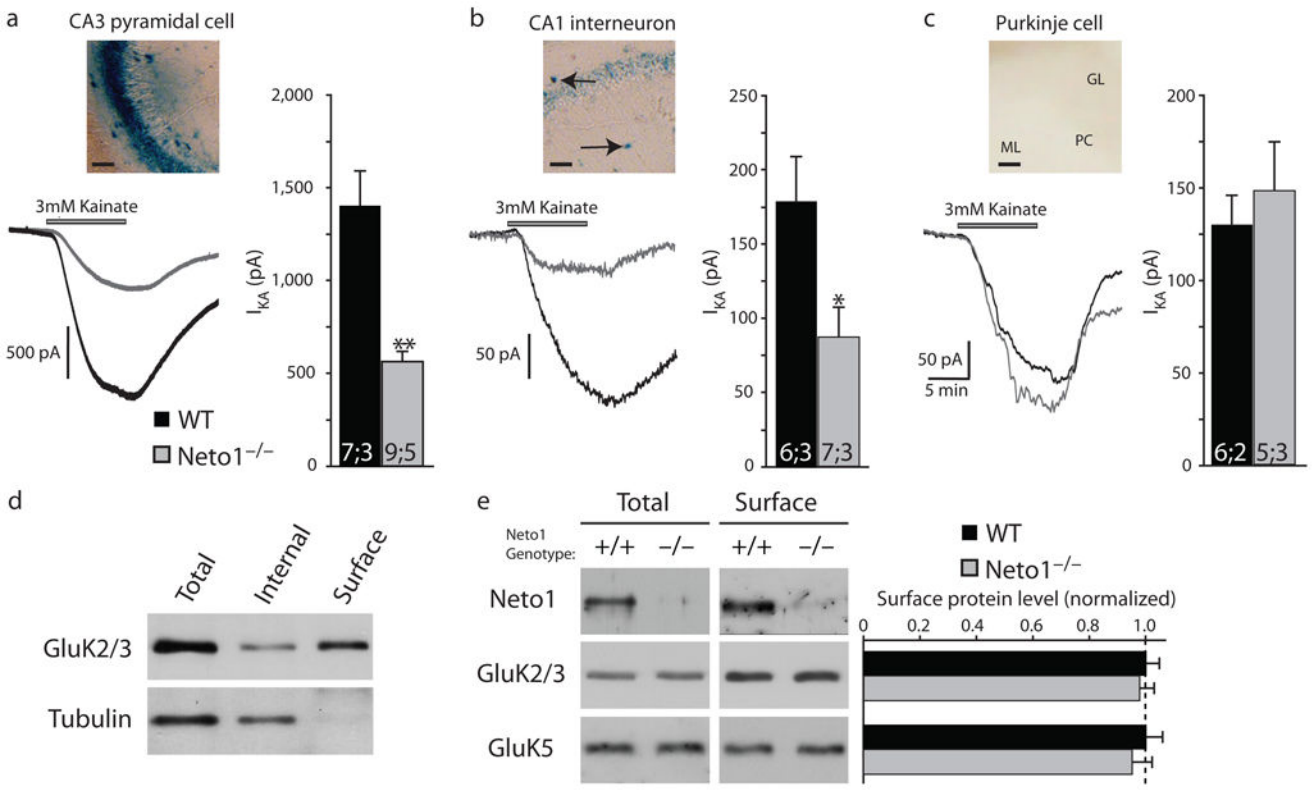

Figure 4.

Neto1 modulates kainate receptor function in the hippocampus. (**a-c**) Representative examples of inward currents elicited by agonist (3 μM kainate) from Neto1-knockout and wild-type littermate mice recorded in the whole-cell voltage clamp configuration in CA3 pyramidal cells (**a**), CA1 *s. radiatum* interneurons (**b**), and cerebellar Purkinje cells (**c**). Kainate-evoked inward currents were recorded in the presence of (in μM) 30 GYKI 53655, 50 d-APV, 100 picrotoxin, and 0.5 TTX. Each bar shows the mean peak current amplitude in each neuron from the numbers of cells;animals indicated. (**d**) To compare cell surface expression of KARs, acute hippocampal slices were prepared and biotinylated with cell-impermeable Sulfo-NHS-SS-biotin. After solubilization, biotinylated proteins were precipitated with Neutravidin-beads to isolate proteins at the cell surface. Most GluK2/3 was detected in the “Surface” fraction, whereas a cytosolic protein, tubulin, was detected in the “Internal” fraction. (**e**) No obvious change in surface expression of GluK2/3 or GluK5 was observed in acute hippocampal slices from wild-type and Neto1-knockout mice (n = 6). Scale bars (a-c): 50 μm. Data are given as mean ± s.e.m.; * $P < 0.05$, * $P < 0.01$.

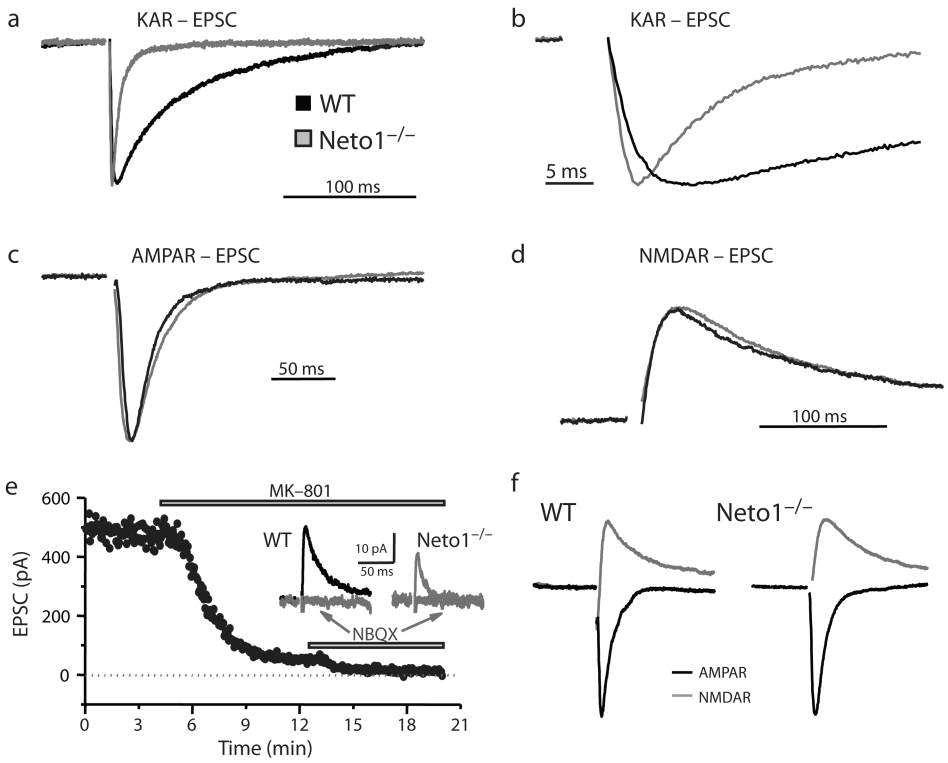

Figure 5.

The slow decay of kainate receptor–mediated synaptic transmission is determined by Neto1. (**a,b**) Representative normalized kainate receptor (KAR)-mediated EPSCs showing faster EPSC decay time constant (tau) (**a**) and rise time (**b**) in Neto1 knockout mice compare to wild littermates. (**c,d**) Representative traces of AMPA receptor (AMPAR)-mediated EPSCs (elicited by stimulation of associational/commissural fibers), and NMDA receptor (NMDAR)-mediated EPSCs (elicited by mossy fiber stimulation) showing no difference between WT and Neto1 knockout littermates. (**e**) Representative example of a KAR/NMDAR experiment. Mossy fiber-evoked mixed KAR and NMDAR responses were recorded at +30 mV in the presence of 30 μM GYKI 53655, 100 μM picrotoxin, and 3 μM CGP 55845. After a baseline was acquired, 50 μM MK-801 was washed in to isolate pure KAR-EPSCs, which were subsequently abolished in the presence of 10 μM NBQX. Inset traces depict the residual KAR-EPSC following MK-801 wash-in for Neto1 knockout and WT littermates. (**f**) Representative normalized AMPAR/NMDAR-EPSCs from wild-type and Neto1 knockout mice.

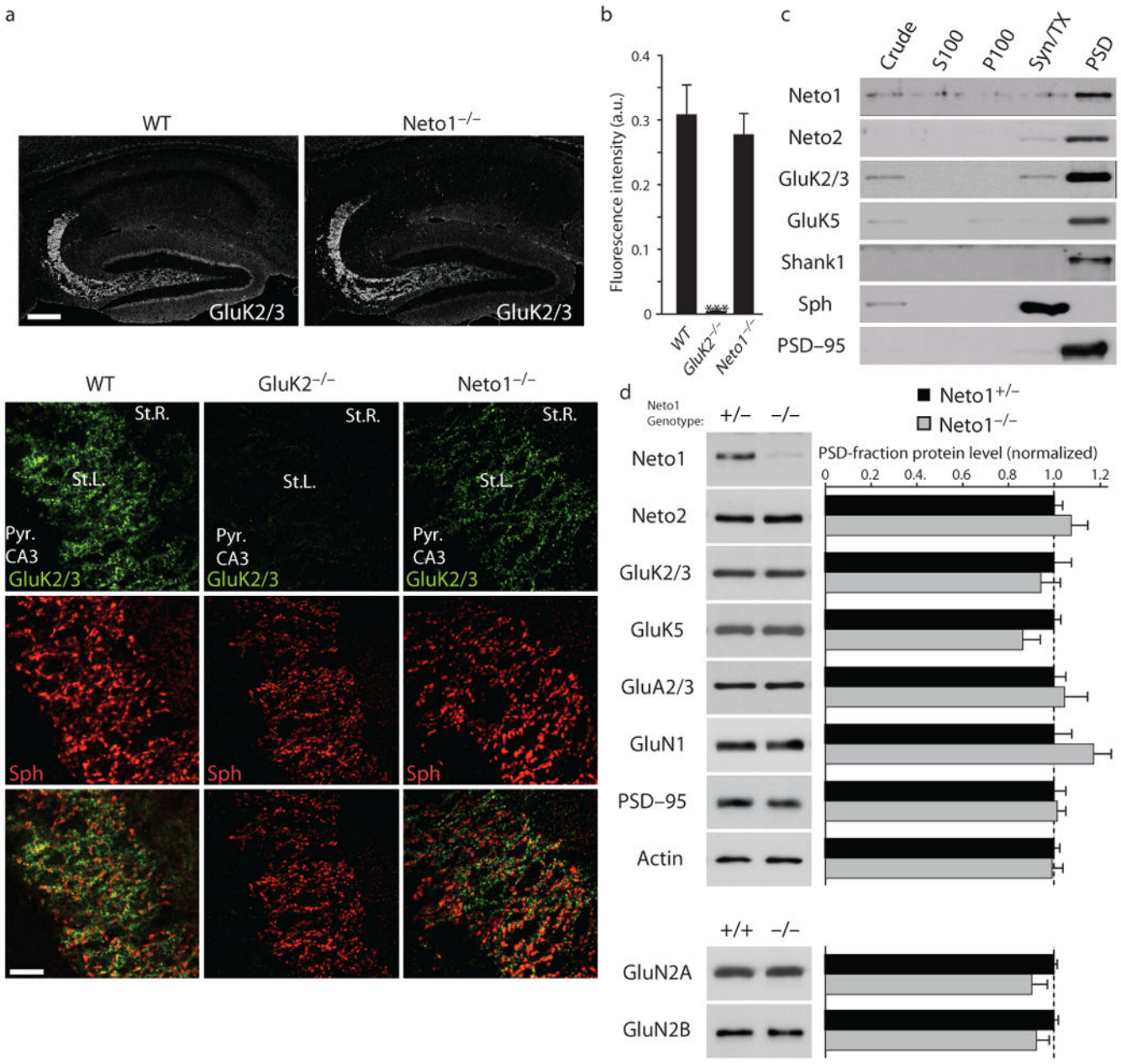

Figure 6.

Localization of kainate receptors in the brain is independent of Neto1 and its PDZ binding domain. **(a)** GluK2/3 protein was observed by immunohistochemistry in *s. lucidum*, and no obvious difference was detected between the wild type (WT) and Neto1-knockout(−/−). Scale bars: 200 μm. High-magnification confocal microscopy in *s. lucidum* showed that GluK2/3 immunoreactivity (green) was unchanged in the Neto1-knockout, but was not detected in the GluK2 knockout (−/−). A presynaptic marker protein, synaptophysin (Sph; red), showed no difference among the three genotypes. Scale bars: 20 μm. (**b**) Relative fluorescence intensity (GluK2/Sph) from randomly selected CA3 areas was measured (n=6). (**c**). Biochemical fractionation of hippocampi showed enrichment of Neto1, Neto2, GluK2/3,

and GluK5 in the PSD fraction together with PSD-95 and Shank1 as markers for the PSD and *s. lucidum* glomerulus-type synapse, respectively. (**d**) Protein expression in the PSD fraction. No change in protein expression of ionotropic glutamate receptors and Neto2 was observed in the Neto1-knockout. For analysis of GluN2A and GluN2B, comparison between wild type (+/+) and knockout littermates is shown (n=4). Data are given as mean ± s.e.m.; * $P < 0.05$, *** $P < 0.005$.

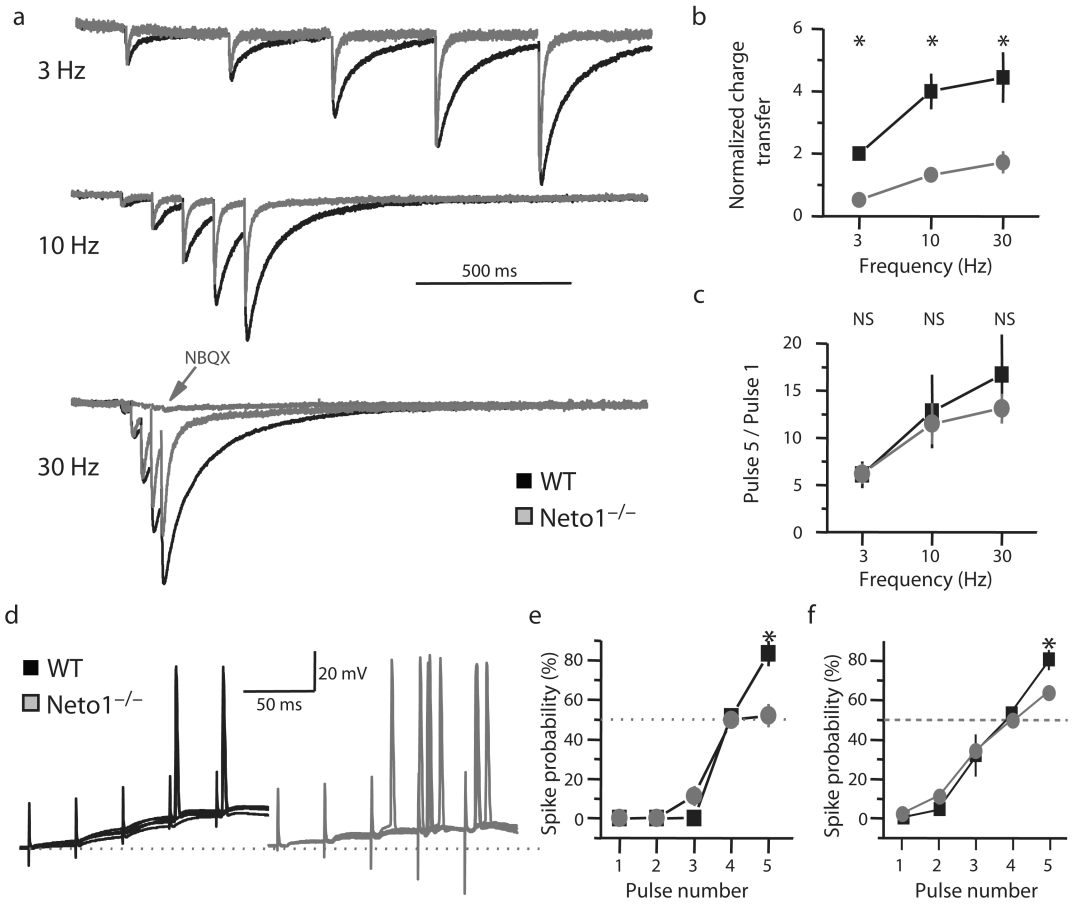

Figure 7.

Neto1 modulates KAR-driven temporal summation and spike fidelity in CA3 pyramidal neurons. (**a**) Neto1 significantly contributes to the charge transfer of KAR-EPSCs elicited by brief bursts (5 pulses) of mossy fiber stimulation at 3, 10, and 30 Hz. Representative averaged traces are normalized to the peak of the first response. (**b**) Summary data indicate a significant attenuation of the KAR-EPCS charge transfer between wild-type and Neto1-knockout littermates. Normalized charge transfer was calculated by integrating the area under the curve for traces that were normalized to the peak amplitude of the first response. (**c**) Presynaptic facilitation is unchanged between wild-type and Neto1-knockout littermates. Pulse 5/Pulse 1 current amplitudes were calculated across the frequency range tested, and no significant difference was observed. (**d**) Neto1 can significantly impact spiking output of CA3 pyramidal cells driven by synaptic KARs. KAR-EPSPs were elicited by short bursts of MF stimulation (5 pulses) while recording from CA3 pyramidal cells in whole-cell current clamp mode. Stimulation intensity was adjusted such that a spike was elicited following the fourth stimulation 50% of the time. (**e**) Summary data of all experiments as in (**d**) (7 cells, 3 animals for WT and KO). (**f**) Even in the absence of glutamate receptor antagonists, spike probability during the fifth pulse was also significantly lower in Neto1 knockout animals than in their WT littermates (6 cells, 3 animals for both genotypes). Data are given as mean ± s.e.m.; * $P < 0.05$.